

# Intranasally Administered S100A9 Amyloids Induced Cellular Stress, Amyloid Seeding, and Behavioral Impairment in Aged Mice

Igor A. Iashchishyn,<sup>†,‡,§</sup> Marina A. Gruden,<sup>‡</sup> Roman A. Moskalenko,<sup>§,∇</sup> Tatiana V. Davydova,<sup>||</sup> Chao Wang,<sup>†</sup> Robert D. E. Sewell,<sup>⊥</sup> and Ludmilla A. Morozova-Roche<sup>\*,†,§</sup>

<sup>†</sup>Department of Medical Biochemistry and Biophysics, Umeå University, Umeå SE-90187, Sweden

<sup>‡</sup>Department of Functional Neurochemistry, P. K. Anokhin Research Institute of Normal Physiology, Moscow 125315, Russia

<sup>§</sup>Department of Pathology, Sumy State University, Sumy 40007, Ukraine

<sup>||</sup>Department of Neuroimmunopathology, Research Institute of General Pathology and Pathophysiology, Moscow 125315, Russia

<sup>⊥</sup>Cardiff School of Pharmacy and Pharmaceutical Sciences, Cardiff University, Cardiff CF10 3NB, United Kingdom

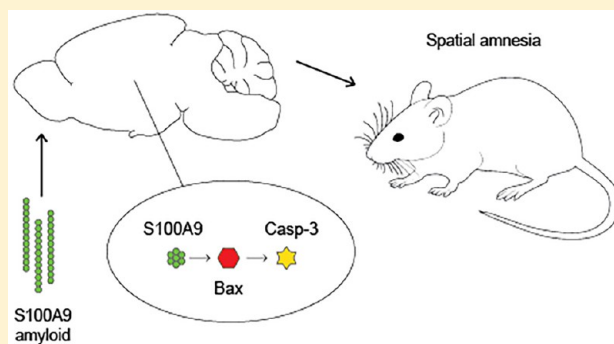
<sup>#</sup>Department of General Chemistry, Sumy State University, Sumy 40007, Ukraine

<sup>∇</sup>Department of Medical Biochemistry and Biophysics, Umeå University, Umeå SE-90187, Sweden

## Supporting Information

**ABSTRACT:** Amyloid formation and neuroinflammation are major features of Alzheimer's disease pathology. Proinflammatory mediator S100A9 was shown to act as a link between the amyloid and neuroinflammatory cascades in Alzheimer's disease, leading together with A $\beta$  to plaque formation, neuronal loss and memory impairment. In order to examine if S100A9 alone in its native and amyloid states can induce neuronal stress and memory impairment, we have administered S100A9 species intranasally to aged mice. Single and sequential immunohistochemistry and passive avoidance behavioral test were conducted to evaluate the consequences. Administered S100A9 species induced widespread cellular stress responses in cerebral structures, including frontal lobe, hippocampus and cerebellum. These were manifested by increased levels of S100A9, Bax, and to a lesser extent activated caspase-3 immunopositive cells. Upon administration of S100A9 fibrils, the amyloid oligomerization was observed in the brain tissues, which can further exacerbate cellular stress. The cellular stress responses correlated with significantly increased training and decreased retention latencies measured in the passive avoidance test for the S100A9 treated animal groups. Remarkably, the effect size in the behavioral tests was moderate already in the group treated with native S100A9, while the effect sizes were large in the groups administered S100A9 amyloid oligomers or fibrils. The findings demonstrate the brain susceptibility to neurotoxic damage of S100A9 species leading to behavioral and memory impairments. Intranasal administration of S100A9 species proved to be an effective method to study amyloid induced brain dysfunctions, and S100A9 itself may be postulated as a target to allay early stage neurodegenerative and neuroinflammatory processes.

**KEYWORDS:** Aged mice, amyloid, apoptosis, BAX, activated caspase-3, cellular stress, learning and memory, neuroinflammation, S100A9



## INTRODUCTION

Ordered protein aggregation, known as amyloid formation, has recently emerged as a universal phenomenon involved in a number of human pathologies including Alzheimer's and Parkinson's diseases, diabetes mellitus, and others.<sup>1</sup> Amyloid is characterized by a generic structure of cross- $\beta$ -sheet in its core, and this structure is common to all amyloid fibrils formed by various structurally unrelated polypeptides both in vivo and in vitro. Amyloids can be deposited in various tissues and organs causing damage due to their hazardous accumulation and cytotoxicity of small self-assembled entities known as amyloid oligomers.<sup>2</sup> It has been demonstrated that a number of

neurodegenerative amyloid illnesses share links with age-dependent changes in the body. The growing elderly population correlates with significant increase in numbers of patients suffering from neurodegenerative conditions and ultimately with increasing social and health care costs. By statistical estimate in 2050, a population of more than 100 million people worldwide will suffer from Alzheimer's disease and that will triple the current number.

**Received:** December 20, 2017

**Accepted:** April 4, 2018

**Published:** April 4, 2018

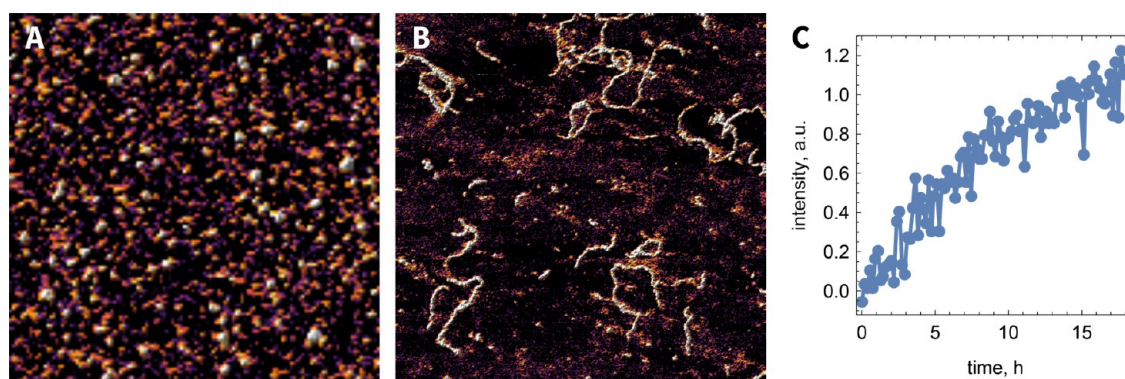


**Figure 1.** Characterization of S100A9 amyloid species. (A, B) AFM height images of S100A9 amyloid oligomers and fibrils, respectively. Size of each image is  $1 \mu\text{m} \times 1 \mu\text{m}$ . (C) Kinetics of S100A9 amyloid formation monitored by thioflavin-T fluorescence assay.

One of the hallmarks of Alzheimer's disease is  $A\beta$  peptide amyloid accumulation. However, increasing evidence has demonstrated that inflammation may also play a crucial role in triggering and promoting neurodegeneration.<sup>3,4</sup> Chronic and acute inflammation associated with traumatic brain injury may fulfill this role and is the subject of intense scrutiny.<sup>5</sup> Epidemiological studies have demonstrated that nonsteroidal anti-inflammatory drugs markedly reduce the age-related prevalence of Alzheimer's disease.<sup>6</sup> Experimental studies have shown that these drugs can slow down amyloid deposition in animal models by mechanisms that still remain poorly understood.<sup>7</sup> Inflammation in Alzheimer's disease is supported by a sharp induction of inflammatory mediators within the brain tissues affected by disease.<sup>8</sup> In general, during  $A\beta$  amyloid plaque formation microglia become activated and recruited to the deposition sites causing microgliosis,<sup>9</sup> although Alzheimer's-type plaques can also be sustained in the absence of microglia.<sup>10</sup> The activated microglia secrete an array of pro- and anti-inflammatory mediators, which may contribute to changes in neuronal calcium homeostasis and further accelerate neuritic and synaptic dysfunction.<sup>11,12</sup>

Among the numerous inflammatory factors and cytokines associated with neuroinflammation here we focus specifically on S100A9 protein, possessing not only pro-inflammatory but also amyloidogenic properties.<sup>13,14</sup> It belongs to the family of S100 proteins, which are characterized by structural homology and the ability to bind calcium ions. They perform signaling functions in numerous inflammation-related conditions, including cancers, autoimmune diseases, and neurodegeneration.<sup>15</sup> Widespread production of S100A9 has been reported in the brain in malaria,<sup>16</sup> cerebral ischemia,<sup>17</sup> and traumatic brain injury,<sup>18</sup> where it may initiate sustainable inflammatory responses and perform cytokine-like functions, affecting inflammatory responses of other cells. Recently, we have demonstrated a critical involvement of S100A9 protein in the amyloid-neuroinflammatory cascade in Alzheimer's disease, where S100A9 exacerbates the aggregation of  $A\beta$  peptide.<sup>14</sup> It has also been shown that in an Alzheimer's disease transgenic mouse model S100A9 expression can be induced by  $A\beta$  peptide, while S100A9 knockdown attenuated memory impairment and reduced amyloid plaque burden.<sup>19</sup> Similarly, in transgenic APP mice, amyloid aggregation of another protein from the S100 family, S100A8, has been shown to precede  $A\beta$  plaque formation and the positive feedback was involved for both S100A8 and  $A\beta$  production.<sup>20</sup> Furthermore, *in vitro* amyloid fibrillation was found to be a property of S100A6

protein from the same family, which can promote amyloid aggregation of superoxide dismutase-1 involved in amyotrophic lateral sclerosis pathology.<sup>21</sup> The amyloid propensity of the S100 protein family is related to the presence of intrinsically disordered sequences in their primary structure, which can be exposed upon loss of structural protection in the native tertiary or quaternary folds and become accessible to amyloid-competent conformations.<sup>22</sup> The amyloid formation of S100A9 can be promoted by a general rise of its concentration occurring during inflammation in the tissue, as reported in Alzheimer's disease<sup>14</sup> and the aging prostate,<sup>23</sup> as well as by S100A9 overexpression in a cell model<sup>24</sup> or in concentrated solutions *in vitro*.<sup>14,25</sup>

Previous studies have shown that amyloid species and other proteinaceous compounds can be delivered to the brain via the nasal route, thus bypassing the blood-brain barrier. The nasal vector has proved to be an efficient route for targeting the brain and evaluating amyloid induced central nervous system and related behavioral dysfunctions following  $A\beta$  peptide administration in rats<sup>26</sup> as well as administration of S100A9 and  $\alpha$ -synuclein amyloid species in mice.<sup>27–29</sup> Nasal delivery to the brain has also been demonstrated for other peptides and proteins such as glycogen, vasopressin, insulin-like growth factor, and insulin.<sup>30–32</sup>

In this study, we administered S100A9 amyloid species via intranasal route in aged mice in order to elucidate their effect on cellular responses and amyloid seeding in the brain tissues in conjunction with behavioral impairment comparable to Alzheimer's-like pathology. Alzheimer's and Alzheimer's-like pathology have been studied intensively using both non-transgenic and transgenic mouse models, which may feature some, but not all Alzheimer's pathologies. A wide range of transgenic Alzheimer's models were generated to monitor disease progression.<sup>19,33–35</sup> However, usage of the transgenic mice could be time-consuming and often uneconomical since it takes months for the animals to develop  $A\beta$  plaques and even longer to show  $A\beta$ -induced synaptic or behavioral abnormalities.<sup>33,36</sup> In addition, the amyloid fibrils deposited in the brain of the transgenic mice may be chemically and morphologically distinct from those accumulated in the Alzheimer's disease brain.<sup>37</sup> Therefore, there are distinct advantages to use nontransgenic mouse models based on the direct active compound administration, such as injection of  $A\beta$  or scopolamine.<sup>38,39</sup> These models may mimic some symptomatic outcomes, such as behavioral abnormalities or exhibit to different degrees  $A\beta$  related molecular and cellular pathology.

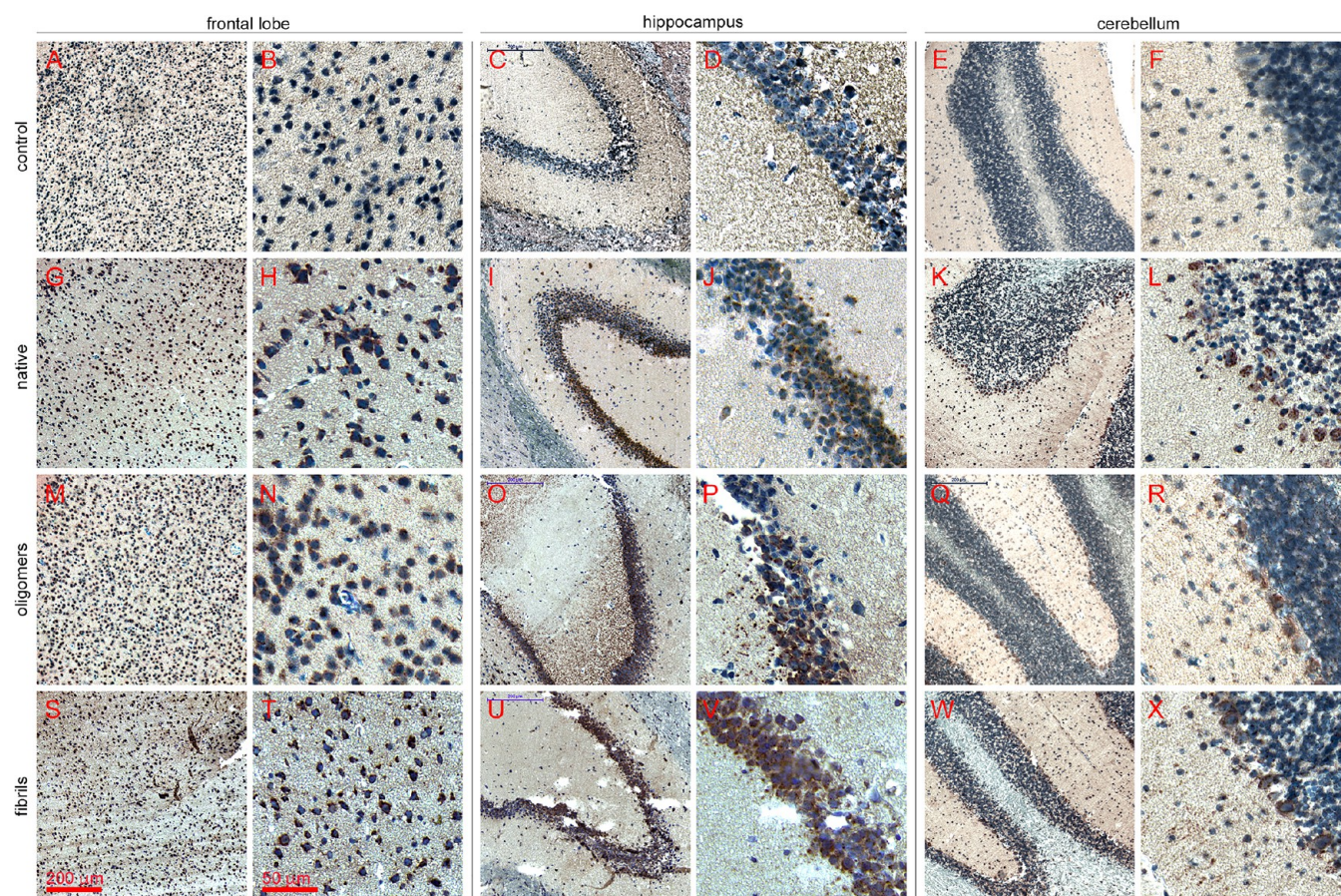


**Figure 2.** Immunohistochemical analysis of mouse brain tissues with S100A9 antibodies. Representative immunohistochemistry with S100A9 antibodies of the brain tissues of animal administered saline vehicle is shown in the first row (A–F), native S100A9 in the second row (G–L), S100A9 oligomeric species in the third row (M–R), and S100A9 fibrils in the fourth row (S–X) (rows counted from top to bottom). Immunohistochemistry of the frontal lobe is shown in columns 1, 2; hippocampus in columns 3, 4; and cerebellum in columns 5, 6 (columns counted from left to right). The broad areas of hippocampus, frontal lobe, and cerebellum are presented in the columns 1, 3, and 5 from left to right (with 200  $\mu\text{m}$  scale bars) and the corresponding magnified areas in the columns 2, 4, and 6 from left to right (with 50  $\mu\text{m}$  scale bars). Blue color corresponds to Mayer's hematoxylin staining, and red-brown color to S100A9 antigen staining.

The present experiments were carried out in order to shed light on the role of S100A9 alone in inducing Alzheimer's-like tissue and behavioral outcomes in contrast to  $A\beta$  peptide, which has been primarily implicated in Alzheimer's disease pathology.

## RESULTS

**Characterization of S100A9 Amyloid Oligomer and Fibrillar Species.** The samples containing S100A9 amyloid oligomers and fibrils were incubated under conditions described in [Methods](#) and collected after 2 and 24 h, respectively. S100A9 amyloid oligomers were characterized by a round-shaped morphology, and some of them were aligned into short stretched protofilaments as assessed by atomic force microscopy (AFM) imaging ([Figure 1A](#)). S100A9 amyloid fibrils were flexible and coiled, reaching a few hundred nanometers in length ([Figure 1B](#)). The presence of some round-shaped oligomers among the fibrillar species could not be excluded, as evident in AFM image ([Figure 1B](#)), that could occur due to fibril breaking and amyloid material recycling.<sup>40,41</sup> However, the majority of species in this sample were fibrillar. The amyloid formation of S100A9 was corroborated also by increasing thioflavin-T fluorescence, occurring when the dye binds specifically to the amyloid species ([Figure 1C](#)). The thioflavin-T fluorescence signal after 2 h incubation, corre-

sponding to the formation of amyloid oligomers, was by ca. 10 times lower than after 24 h, when thioflavin-T signal has reached plateau level and amyloid fibrils were formed ([Figure 1C](#)).

**Immunohistochemical Analysis of Mouse Brain Tissues.** After intranasal administration of S100A9 species, the location of S100A9 antigens in the mouse brain tissues, including the frontal lobe, hippocampus and cerebellum areas, was analyzed by using immunohistochemistry ([Figure 2](#)). Four groups of animals were subjected to dosing protocol as described in [Methods](#). In all studied brain tissues, cell nuclei were contrasted by hematoxylin staining. Even in the control group some S100A9 immunopositive cells were present in all studied brain regions, which may be related to their age (12 months old) and age-related tissue changes<sup>19</sup> ([Figure 2A–F](#)). In general, S100A9 immunopositive cells were found in both S100A9 treated and control animals and they were located within the III–V cell layers of the frontal lobe, morphologically resembling pyramidal, grain, and ganglion neurons ([Figure 2B, H, N, T](#)); in the pyramidal layer of the archicortex Ammon's horn of the hippocampus ([Figure 2D, J, P, V](#)) and in the cerebellum corresponding to Purkinje cells ([Figure 2F, L, R, X](#)).

Sequential immunohistochemistry with S100A9 and NeuN antibodies was conducted on the same brain tissues of mouse

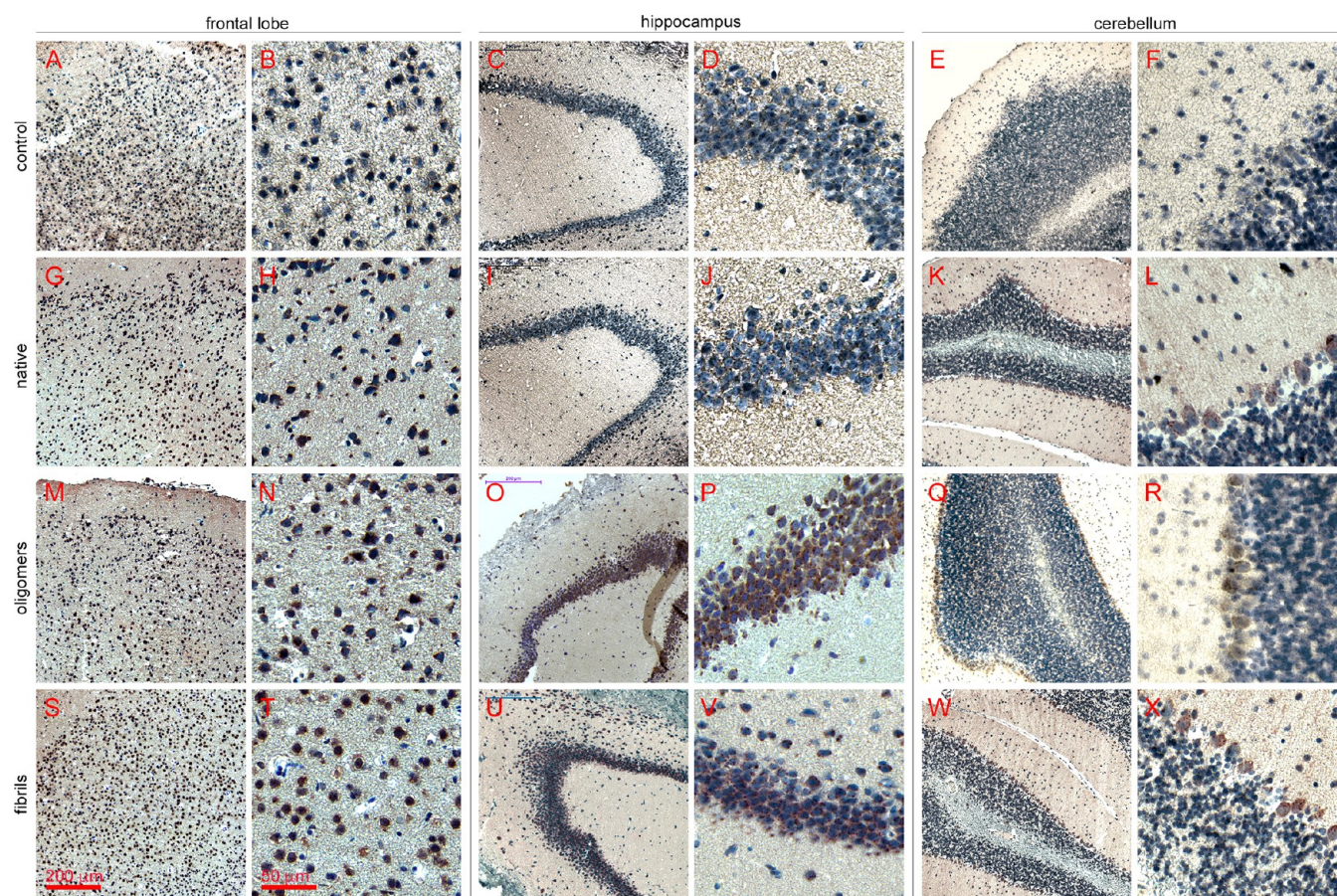


**Figure 3.** Immunohistochemical analysis of mouse brain tissues with Bax antibodies. Designation of images and color presentations are as in Figure 2.

treated with S100A9 amyloid fibrils in order to examine if S100A9 is present in neuronal cells (Figure S1). We have observed clear colocalization of S100A9 and NueN staining (overlapping of immunostaining patterns) as shown in representative images of neuronal cells in the frontal lobe, and the same observation were made in the hippocampus and cerebellum, confirming that S100A9 is indeed expressed by neuronal cells. The same immunostaining pattern was observed in other groups of S100A9 treated mice.

Immunohistochemistry with Bax (Figure 3) and activated caspase-3 (Figure S2) antibodies was conducted in a similar set up and revealed similar patterns in all studied brain structures as the immunostaining with S100A9 antibodies (Figure 2). This indicates that proapoptotic markers were also induced in the brain tissues immunopositive for S100A9. Specifically, the colocalization of S100A9 and activated caspase-3 immunostaining patterns was observed in all three studied brain areas of mouse treated with S100A9 amyloid fibrils by using sequential immunohistochemistry with corresponding antibodies (Figure S3), indicating that both antigens may be produced within the same cells.

**Quantification of Immunopositive Cells in Mouse Brain Tissues.** In order to estimate the relative effect of administered S100A9 amyloid species on the cell stress in the mouse brain tissues compared to controls, the cells immunopositive for S100A9, Bax and activated caspase-3 were counted in six randomly selected areas in each brain structure. The counts are presented by box-plots, where each point corresponds to an average of the counts from six random

areas (Figure 4). The number of S100A9-immunopositive cells significantly increased in the frontal lobe and hippocampus upon administration of all S100A9 species, containing native protein, oligomers and fibrils, respectively (Figure 4A, B). The largest increase of S100A9 immunopositive cells was observed in these tissues upon administration of S100A9 oligomeric species with the increase of median values by two and three folds in the frontal lobe and hippocampus, respectively. In the cerebellum, the amounts of S100A9 immunopositive cells in all treated groups were generally lower compared to those in the frontal lobe and hippocampus, however these levels were still significantly higher than in controls (Figure 4A–C).

Significant increase in the numbers of Bax immunopositive cells was observed in the frontal lobe of mice treated with all S100A9 species compared to controls with the largest increase corresponding to the group administered amyloid oligomers (Figure 4D). In the hippocampus, the most pronounced increase in the level of Bax immunopositive cells was observed in mice administered S100A9 oligomers and fibrils (Figure 4E). Upon administration of the native and oligomeric S100A9 species, the amounts of Bax positive cells in the cerebellum were very close to those in control group, except for a significant increase in the group treated with S100A9 fibrils (Figure 4F). The changes in the S100A9 and Bax immunopositive cell levels in the mouse brain tissues broadly resemble each other (Figure 4). This suggests that induction of S100A9 and Bax occurred via similar mechanisms and the frontal lobe is the most affected by the administration of S100A9 species.

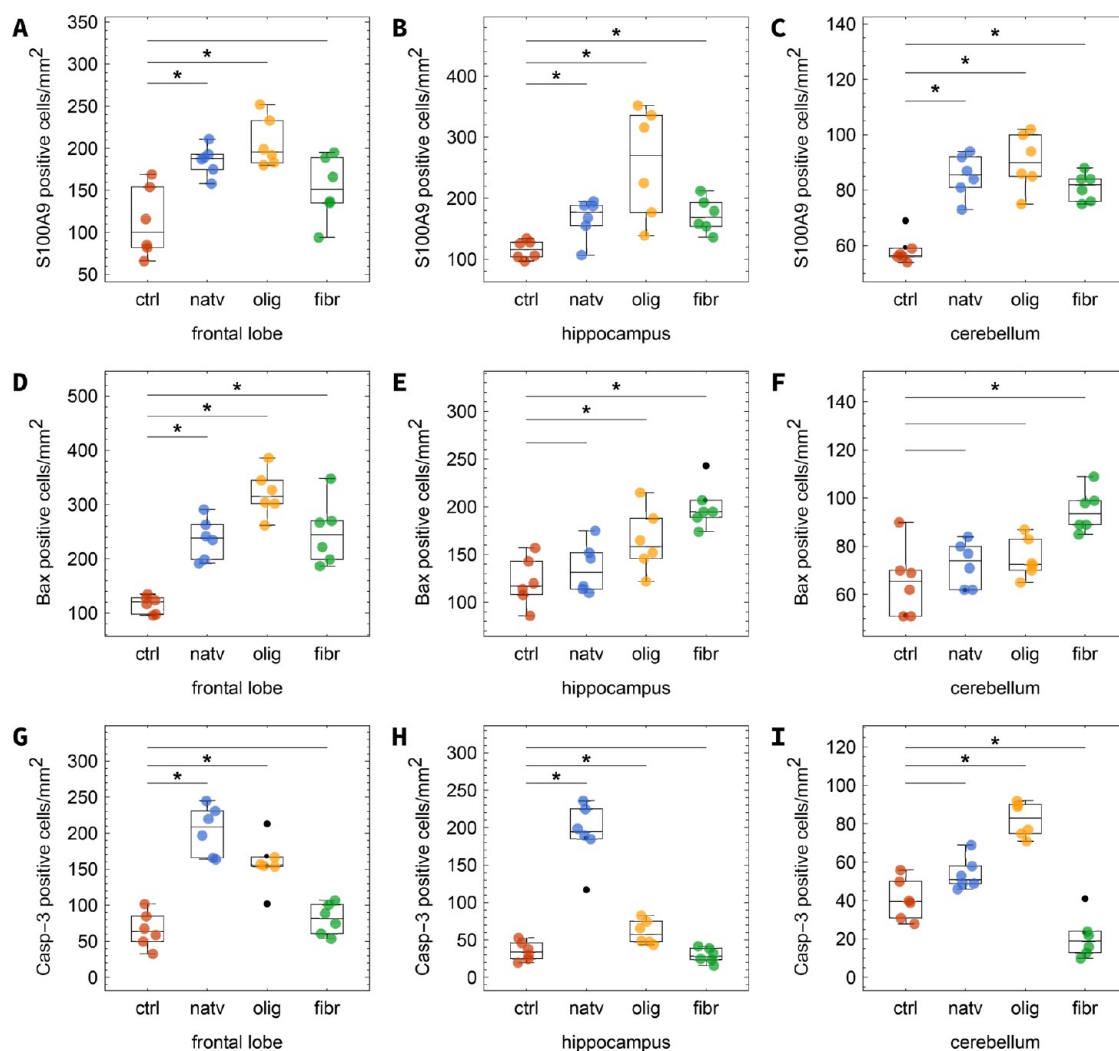


**Figure 4.** Quantification of S100A9, Bax and activated caspase-3 immunopositive cells in mouse brain tissues. Quantification of immunopositive cells reactive with S100A9 (A–C), Bax (D–F), and activated caspase-3 (G–I) antibodies. Counts of immunopositive cells per square millimeter are shown along the y-axis. Counts of immunopositive cells in the frontal lobe are shown in the left column (A, D, G), in the hippocampus in the central column (B, E, H), and in the cerebellum in the right column (C, F, I). Data are presented by box plots with the corresponding data points per each animal; central line represents median, and whiskers represent q1 and q4 quartiles. Outliers are shown by black dots. Cell counts in the control group are shown in red, in the group treated with native S100A9 in blue, in the group treated with oligomeric S100A9 in yellow, and in the group treated with fibrillar S100A9 in green. \* $p < 0.05$  is compared to control group.

The highest levels of activated caspase-3 immunopositive cells were observed in the frontal lobe and hippocampus of mice treated with native S100A9 compared to controls (Figure 4G, H). The administration of S100A9 oligomers also led to significant increase of the number of activated caspase-3 immunopositive cells both in the frontal lobes and hippocampus (Figure 4G, H); however, the S100A9 fibrillar species did not induce activated caspase-3 in either the frontal lobe or hippocampus. In the cerebellum, the number of activated caspase-3 positive cells increased in the group administered oligomeric S100A9, while in other groups those levels remained close to controls (Figure 4I). Thus, the pattern of activated caspase-3 induction in the mouse brain areas deviates from those of S100A9 and Bax. However, in all treated animal groups, the frontal lobe is the most susceptible region to the administration of S100A9 species as shown by a drastic rise of the levels of S100A9, Bax, and activated caspase-3 immunopositive cells, while the cerebellum is the least susceptible area (Figure 4).

**Localization of A $\beta$  and Amyloid Oligomers in Mouse Brain Tissues.** Sequential immunohistochemistry with A $\beta$ , S100A9 and oligomer specific A11 antibodies was conducted to examine the localization of these antigens relative to each other in the mouse brain tissues after administration the samples containing S100A9 fibrils (Figure 5). We have observed S100A9 positive cells in all studied brain areas as indicated above (Figures 2, 4). The deposits of A $\beta$  peptide were found only in the blood vessels in the frontal lobe, hippocampus, and cerebellum of the S100A9 treated mice (Figure 5A, E, I) as well as in control animals (Figure S4A, D, G). However, S100A9 was not found in these blood vessels, but only in neuronal cells in the surrounding tissues, indicating that S100A9 and A $\beta$  are not colocalized.

The A11 immunopositive staining was observed in all studied brain areas in the group of mice treated with the S100A9 fibrillar species compared to controls (Figure 5B, F, J). The round-shaped inclusions of proteinaceous material reactive with A11 antibodies were well spread in the brain tissues of S100A9

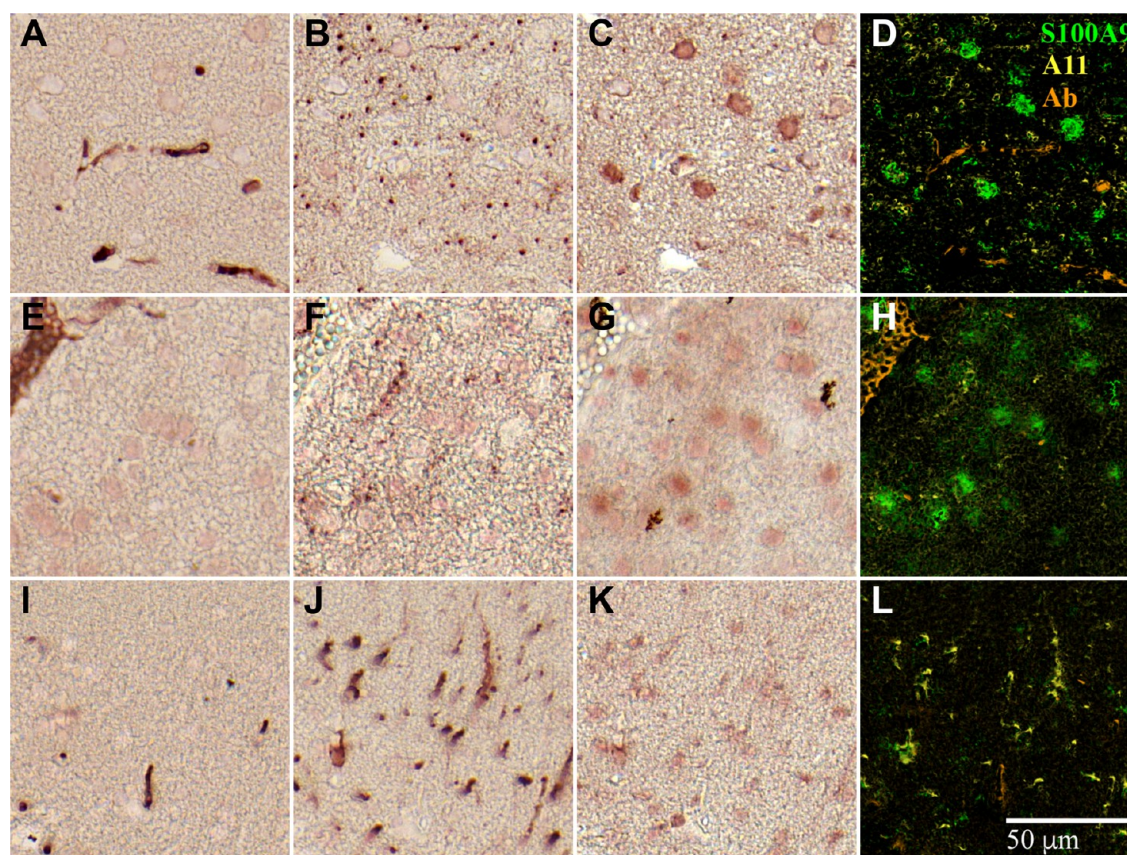


**Figure 5.** Localization of  $A\beta$ , S100A9, and amyloid oligomers in mouse brain tissues. Immunohistochemistry with  $A\beta$  (A, E, I), A11 (B, F, J), and S100A9 (C, G, K) antibodies of the brain tissues of mouse administered S100A9 fibrils. Immunohistochemistry of the frontal lobe tissues is shown in (A–D); hippocampus in (E–H), and cerebellum in (I–L). Superposition of corresponding immunostainings in pseudocolors (D, H, L): S100A9 staining is shown in green, A11 in yellow, and  $A\beta$  in orange. Scale bar is 50  $\mu\text{m}$ .

treated animals, while the brain structures of control group were characterized by complete lack of A11 antibody reactivity (Figure S4B, E, H). However, neither in the frontal lobe nor in other studied brain regions the immunostaining patterns of S100A9 and A11 were fully overlapped as well as there was no overlapping of A11 immunostaining with  $A\beta$  peptide accumulations found in blood vessels (Figures 5 and S4). Since S100A9, but not  $A\beta$ , was shown to be produced by neuronal cells (Figure S1), this suggests that in some cells or extracellularly S100A9 may be present at the levels exceeding critical concentration and sufficient for spontaneous self-assembly into amyloid oligomers, especially if this process is further exacerbated by administered amyloid species.<sup>25,42</sup> Clearly,  $A\beta$  was not a leading amyloidogenic peptide aggregating in the mouse brain tissues, as it was found only in the blood vessels (Figure 5A, E, I). Its presence in the blood vessels is more likely related to mouse age,<sup>19,43</sup> since the same pattern was observed both in animals treated with S100A9 fibrils and in controls.

#### Mouse Performance in Passive Avoidance Test.

Results of the passive avoidance test, to which all four animal groups were subjected, are presented by box plots in Figure 6. Remarkably, all mouse groups treated with S100A9 species showed statistically significant increase in training latencies (Figure 6A) and decrease in retention latencies compared to controls (Figure 6B). Furthermore, we have estimated the magnitude of the observed effect<sup>44</sup> in addition to its statistical significance. We evaluated the effect size by using Cliff's delta

( $\delta$ ) and its 95% confidence intervals (Figure 6C).<sup>45</sup> Cliff's delta is defined to range from  $-1$  to  $1$ , reflecting the extent to which one distribution tends to generally lie above or below another.<sup>45</sup> We used here the following scale for the effect size:  $0.1 < \delta < 0.3$  corresponded to a small effect,  $0.3 < \delta < 0.5$  to a medium effect, and  $0.5 < \delta < 1.0$  to a large effect.<sup>46</sup> The effect sizes for the training (0.48, 95% CI 0.11, 0.74) and retention ( $-0.46$ , 95% CI  $-0.08$ ,  $-0.77$ ) latencies for the group treated with native S100A9 were medium. Importantly, the effect sizes for both latencies in the groups treated with S100A9 amyloid oligomers and fibrils were large. Specifically, the effect sizes for the training latencies in the groups treated with amyloid oligomers and fibrils were 0.9, 95% CI 0.56, 0.98 and 0.71, 95% CI 0.35, 0.87, respectively. The effect sizes for the retention latencies in the same groups were 0.73, 95% CI 0.38, 0.98 and 0.78, 95% CI 0.52, 0.99, respectively. These clearly demonstrate that the animals treated with S100A9 species, especially amyloid oligomers and fibrils, displayed impediments both in training and subsequent memory retention, reflecting impairment of their fear-aggravated memory formation.

## DISCUSSION

The proinflammatory mediator S100A9 has been identified as an important contributor to Alzheimer's disease pathology<sup>47,48</sup> and inflammation-dependent aging.<sup>49</sup> Recently, we have demonstrated that S100A9 serves as a critical link between the neuroinflammatory and amyloid cascades in Alzheimer's disease, since it acts as both a proinflammatory mediator

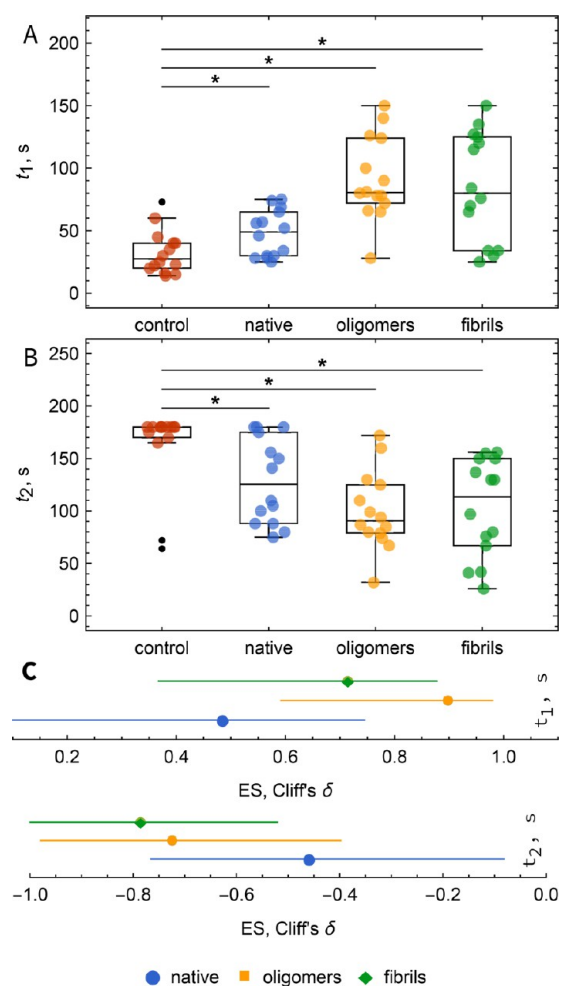


**Figure 6.** Effects of S100A9 species administration on mouse behavior in passive avoidance test. (A) First day training latencies ( $t_1$ ), (B) second day retention latencies ( $t_2$ ), and (C) effect sizes (Cliff's delta) for training and retention latencies in passive avoidance test. The values of latencies are presented by box plots with the corresponding data points; central line represents median, and whiskers represent q1 and q4 quartiles. Outliers are shown by black dots. Data points corresponding to the control group are shown in red, to the group treated with native S100A9 in blue, to the group treated with oligomeric S100A9 in yellow, and to the group treated with fibrillar S100A9 in green. \* $p < 0.05$ .

involved in the damage associated molecular patterns and a highly amyloidogenic protein.<sup>14</sup> In the latter capacity, S100A9 coaggregates together with  $A\beta$  peptide into amyloid fibrils, leading to amyloid plaque formation in the brain tissues, while S100A9 amyloid oligomers exhibit cellular toxicity as demonstrated in *in vitro* experiments. Interestingly, in conjunction with  $A\beta$  peptide S100A9 can be used as a robust diagnostic marker of Alzheimer's disease pathology already at a very early stage of mild cognitive impairment,<sup>50</sup> which further emphasizes its involvement in disease development. Furthermore, in the transgenic Tg2576 mouse model the knockdown of S100a9 expression had improved the cognition decline of Tg2576 mice as assessed by their performance in the water maze task and reduced their amyloid plaque burden.<sup>19</sup> Similarly, a transgenic model of Alzheimer's disease produced by cross-breeding the Tg2576 mouse with the S100A9 knockout mouse displayed an increased spatial reference memory in the Morris water maze and Y-maze tasks as well

as decreased  $A\beta$  neuropathology.<sup>51</sup> These findings suggest that S100A9 in its own right plays an essential role in development of Alzheimer's pathology. Understanding S100A9 multifaceted properties and mechanisms of actions is still in its infancy; however, this knowledge is critical since S100A9 can be used as a therapeutic target in Alzheimer's disease treatment.

By using noninvasive intranasal administration of S100A9 in its native and amyloid forms to aged mice, we have examined their effects on the cellular stress and apoptotic pathway initiation as well as on amyloid seeding in different cerebral structures relevant to fear aggravated memory formation. The pathological outcomes observed in the brain tissues were related to the symptomatic behavior of experimental animals manifested in the training and retention latency changes in the fear aggravated passive avoidance memory test.

It is noteworthy that repetitive 14 day administration of S100A9 native or amyloid species incited substantial cellular stress in the frontal lobe and hippocampus, manifested in increased amounts of the S100A9, Bax, and to a lesser extent of activated caspase-3 immunopositive cells in these areas. The observed cellular responses to S100A9 species can be related both to (1) the signaling properties of native S100A9 able to activate RAGE and TLR-4 receptors and elevate the intracellular level of proinflammatory cytokines<sup>13,52,53</sup> and (2) the cytotoxic and stress inducing properties of amyloid species.<sup>14,54</sup>

The S100A9 oligomeric samples were very potent inducers of intracellular S100A9 and Bax levels both in the frontal lobe and hippocampus (Figures 2–4). In the hippocampus, the sample containing S100A9 amyloid fibrils produced an even more pronounced effect on Bax induction, which could be due to potential fibrillar fractionation and secondary seeding of amyloid oligomers.<sup>41</sup> Interestingly, it has been shown that RAGE activation may occur via binding of monomeric and fibrillar forms of  $A\beta$  and  $\beta$ -sheet fibril structures,<sup>55,56</sup> which does not exclude the possibility that S100A9 amyloids, via their generic amyloid conformational epitope,<sup>57</sup> can also interact with RAGE, inducing activation of the signaling pathways. Moreover, it has been shown recently that S100A9 fibrils provide a priming signal to activate the NLRP3 inflammasome, which causes the release of proinflammatory cytokines such as IL-1B and IL-18.<sup>58</sup> However, in our experiments, the most pronounced effect on intracellular activated caspase-3 induction was produced by native S100A9 in its proinflammatory mediator capacity. Notably, in the cerebellum, the levels of S100A9, Bax, and activated caspase-3 immunopositive cells were low in all treated and control mouse groups, indicating that this area was less susceptible to the effects incited by intranasal S100A9 administration. Importantly, S100A9 was detected specifically in neuronal cells in all studied brain structures as revealed by colocalization of S100A9 and NeuN immunostaining in sequential immunohistochemistry experiments (Figure S1), though S100A9 is also known to be produced in microglial cells.<sup>53</sup>

Since S100A9 is a highly amyloidogenic protein, the administration of S100A9 amyloid species was characterized by amyloid oligomerization in the brain tissues of the S100A9 treated animals compared to controls (Figures 5 and S4). The immunopositive staining pattern with A11 amyloid oligomeric antibodies was observed in all studied brain areas in the treated mice. It is important to note that, among the two amyloidogenic polypeptides associated with Alzheimer's pathology, S100A9 but not  $A\beta$  was a major culprit, since  $A\beta$  was found only in the blood vessels (Figures 5 and S3). Though

both A $\beta$ 40 and A $\beta$ 42 do not form amyloid plaques in wild type mice during their life span, Fung et al.<sup>59</sup> have shown that mouse A $\beta$ 40 and A $\beta$ 42 are as amyloidogenic as human A $\beta$ 40 and A $\beta$ 42 and interspecies A $\beta$  aggregates and fibers are readily formed in vitro. These aggregates are also more stable than homogeneous human fibers.<sup>59</sup> The presence of three amino acid substitutions in the N-terminal part of mouse A $\beta$  do not prevent it from amyloid aggregation and coaggregation with human counterpart. It was suggested also that mouse A $\beta$  may contribute to the amyloid plaque formation in the transgenic mouse, though its quantity is 10–100 times lower than human A $\beta$ .<sup>59</sup> In our experiments, we have decoupled S100A9 effect on the mouse brain tissue from the A $\beta$  pathology by using wild type mice and demonstrated that S100A9 can induce amyloid oligomerization in the brain tissues by its own (Figure 5). In wild-type aged mice A $\beta$  was found only in the blood vessels of both control and treated animals, possibly due to aging, but it was not reactive with amyloid oligomer specific antibodies (Figure 5). It is also notable that amyloid oligomers self-assembled in the mouse brain tissues, due to their inherent cytotoxicity, may provide a positive feedback to the elevated cellular stress level exacerbating it further.

Importantly, the elevated cellular levels of S100A9, Bax, and activated caspase-3 as well as amyloid oligomerization induced in the brain tissues correlated with the behavioral outcome disclosed as significantly increased training and decreased retention latencies observed in the passive avoidance tests for the S100A9 treated groups (Figure 6). Remarkably, the effect size in the behavioral tests was moderate already in the group treated with native S100A9, while the effect sizes were large in the groups administered both S100A9 amyloid oligomers and fibrils. This indicates that the mouse brains were susceptible to the damaging effect of amyloid species and this effect was directly translated into the memory impairments. It is noteworthy that the S100A9 level in human CSF is already perturbed at the stage of mild cognitive impairment, long preceding Alzheimer's disease development, sizable Alzheimer's-related plaque formation, and neuronal loss.<sup>50</sup> The present results indicate that the cellular stress and amyloid oligomerization induced by S100A9 could be important factors triggering the memory impairment in wild type mouse model lacking amyloid plaques.

In conclusion, intranasal administration of S100A9 native and amyloid species induced significant stress responses along with amyloid oligomerization not only locally, but across distant areas of the brain tissues, which ultimately interfered with mouse behavior, provoking significant memory impairment in the passive avoidance test. Since both the tissue and behavioral responses occurred without any noticeable involvement of A $\beta$  amyloid aggregation typical of Alzheimer's disease, this may well signify a critical role of proinflammatory and amyloidogenic S100A9 protein in eliciting Alzheimer's-like pathology and symptoms. It might be further postulated that inflammatory pathways and S100A9 in particular can be used as prospective targets for therapeutic interventions aimed at allaying neurodegenerative and neuroinflammatory processes at a very early stage. In addition, nasal administration of S100A9 species proved to be a compelling method for studying the brain dysfunctions induced by biologically active compounds with amyloid properties, while possessing the advantages of being noninvasive and easy to apply.

## METHODS

**S100A9 and Its Amyloid Species.** S100A9 was expressed in *E. coli* and purified as described previously.<sup>60</sup> Its concentration was determined by measuring optical absorbance at 280 nm. The extinction coefficient was  $\epsilon_{280} = 0.53 \text{ (mg/mL)}^{-1} \text{ cm}^{-1}$ . S100A9 amyloid species were produced upon incubation at 2 mg/mL concentration in PBS buffer, pH 7.4 and 37 °C, using continuous agitation at 600 rpm (Eppendorf Thermomixer Compact). The specimens containing predominantly amyloid oligomers were collected after a 2 h incubation, and the fibrillar species were produced after 24 h. Subsequently, both S100A9 oligomeric and fibrillar samples were lyophilized. They were reconstituted in PBS buffer directly prior administration to mice.

**Thioflavin T Fluorescence Assay.** Thioflavin-T fluorescence assay was performed by adding 20  $\mu\text{M}$  thioflavin-T to S100A9 solutions kept on ice and then pipetted into 96-well plates. Thioflavin-T fluorescence was measured by using a Tecan F200 Pro plate reader, using an excitation filter at 450 nm and an emission filter at 490 nm.

**AFM Imaging.** AFM imaging was carried out by using a BioScope Catalyst AFM (Bruker) in the peak force mode in air at a resolution of  $256 \times 256$  pixels. Amyloid samples were deposited on the surface of a freshly cleaved mica (Ted Pella) for 15 min, washed three times with 100  $\mu\text{L}$  of deionized water, dried at room temperature, and then subjected to AFM analysis.

**Subjects.** Fifty-six adult male C57Bl/6 mice were subjected to experimental procedures. The animals were ca. 12 months old and weighted  $31.1 \pm 1.0$  g. The animals were group-housed on a 12:12 light–dark cycle at 21 °C and 50% humidity with access to food and water ad libitum.

**Dosing Protocol.** Mice were divided into 4 groups of 14 animals per group for a 14 day intranasal dosing protocol.<sup>29,31</sup> The control group was administered 8  $\mu\text{L}$  of saline vehicle daily, and the three experimental groups received 8  $\mu\text{L}$  of saline solution containing 15.0  $\mu\text{g}$  (0.48 mg/kg daily dose) of the following S100A9 species: (1) native protein, (2) amyloid oligomers, and (3) amyloid fibrils. On completion of the 14 day protocol (i.e., on days 15–16), all animal groups underwent behavioral testing. The next day (i.e., on day 17) after these procedures, animals were sacrificed and their brain tissues were fixed in fresh cold 4% paraformaldehyde in PBS, dehydrated in ethanol, cleared in toluene, and embedded in paraffin for subsequent immunohistochemical analyses.

**Behavioral Test.** One-trial step-through passive avoidance test was carried out after training in a PACS-30 two-way shuttle box (Columbus Instruments) as described previously.<sup>61,62</sup> The apparatus consisted of a rectangular chamber divided into two compartments. One compartment was lit by an overhead light stimulus, while the other remained in darkness. They were separated by an automatic guillotine door, and each compartment had a grid floor, through which foot-shock could be delivered. Mouse memory was assessed by the time for a performance measure to occur, i.e., in latency. In our experiments, latencies corresponded to the times required for animals to enter a dark compartment. Briefly, each individual animal was initially introduced into the light compartment. During a habituation period, mice were allowed to freely explore the box for 5 min with an open intercompartment door and subsequently they were returned to their home cage. On the training day, each animal was placed into the lit compartment facing away from the dark one and allowed to explore it for 30 s. The guillotine door was then lifted and upon animal entry into the dark compartment with all four paws plus the tail the guillotine door was closed. The entry time was recorded from the time when the door was lifted. The entry time on the training day or a training latency ( $t_1$ ) was measured. Following a period of 3 s after guillotine door closure, an inescapable foot-shock of 0.5 mA and 3 s duration was delivered and 30 s later each mouse was removed to its home cage. Animals, which did not enter the dark compartment within 180 s, underwent another session of training on the same day. The same test was carried out 24 h after passive avoidance training, and the one-trial step-through latency defined as a retention latency ( $t_2$ ) was



recorded. An increase in training latency and decline in retention latency signified impaired memory in the task.<sup>61,62</sup>

**Immunohistochemistry.** Paraffin embedded mouse brain tissues were microtome sectioned to 3–4  $\mu\text{m}$  thick slices. Single and sequential immunohistochemistries on the same tissue sections were performed as described previously<sup>63</sup> with some modifications.<sup>64</sup> The following primary antibodies were used:  $A\beta$  (mouse monoclonal, ab11132, 1:100, Abcam), S100A9 (rabbit polyclonal, sc-20173, 1:100, Santa Cruz Biotechnology), A11 (rabbit polyclonal, 1:200, gift from Professor Rakez Kaye<sup>57</sup>), NeuN (mouse monoclonal, MAB377, 1:100, Millipore), activated caspase-3 (rabbit polyclonal, ab13847, 1:50, Abcam), and Bax (rabbit polyclonal, sc-526, 1:100, Santa Cruz Biotechnology). Anti-mouse (MP-7402) and anti-rabbit (MP-7401) IgG peroxidase reagent kits (Vector Laboratories) were used as secondary antibodies. The tissues were scanned by using a Panoramic SCAN slide scanner 250 (3D Histech).

**Cell Counting.** Immunopositive cells were counted in six randomly selected circular regions (1 mm diameter each) in the frontal lobe, hippocampus, and cerebellum, respectively, in six mouse brain tissues per group by using a Panoramic Viewer (3DHistech Ltd.). The cell counts were presented by box plots with corresponding data points.

**Data Analysis.** Statistical data analysis was performed by using a Wolfram Mathematica 11 package. Since there were deviations (Shapiro–Wilk test) from the normal distribution in all data sets, nonparametric methods such as Mann–Whitney test and bootstrap were applied as major statistical tools.<sup>65,66</sup> We used the combination of the standardized effect size and associated confidence intervals to assess: (1) the magnitude of an effect of interest, i.e., the changes in the training or retention latencies, respectively, in S100A9 treated groups compared to controls and (2) the precision of the estimate of such changes. Such approach enables us to conclude on the biological importance of the observed effects, rather than merely resorting to statistical significance defined by  $p$ -values.<sup>44</sup>

Cliff's delta was used as a measure of the effect size due to non-normality of the data distributions.<sup>45</sup> Its 95% confidence intervals were calculated by a nonparametric version of corrected and accelerated bootstrap method with 10 000 replications.<sup>65,66</sup>

**Ethics Statement.** All experimental procedures were carried out in accordance with the National Institute of Health Guide for the Care and Use of Laboratory Animals (NIH Publications No. 80-23, revised 1996) and the European Communities Council Directive of 24 November 1986 (86/609/EEC) for care and use of laboratory animals. They were also approved by the Animal Care and Use Committee of the P. K. Anokhin Institute of Normal Physiology, Russian Academy of Medical Science.

## ■ ASSOCIATED CONTENT

### 📄 Supporting Information

The Supporting Information is available free of charge on the ACS Publications website at DOI: 10.1021/acscchemneuro.7b00512.

Representative sequential immunohistochemistry with S100A9 and NeuN antibodies of S100A9 treated mouse brain tissues; immunostaining of the mouse brain tissues with activated caspase-3 antibodies; sequential immunohistochemistry with S100A9 and activated caspase-3 antibodies of S100A9 treated mouse brain tissues; and sequential immunohistochemistry with  $A\beta$ , A11, and S100A9 antibodies of control mouse brain tissues (PDF)

## ■ AUTHOR INFORMATION

### Corresponding Author

\*E-mail: ludmilla.morozova-roche@umu.se.

### ORCID

Igor A. Iashchishyn: 0000-0002-1691-9025

Robert D. E. Sewell: 0000-0003-1702-5100

Ludmilla A. Morozova-Roche: 0000-0001-5886-2023

### Author Contributions

I.A.I., M.A.G., and R.A.M. contributed equally to the work. L.A.M.-R. acquired funding. L.A.M.-R., M.A.G., and R.D.E.S. conceptualized the project. T.V.D., R.A.M., and C.W. conducted the investigation. I.A.I. conducted data curation, formal analysis, and visualization. I.A.I. and L.A.M.-R. created original manuscript. I.A.I., L.A.M.-R., M.A.G., and R.D.E.S. reviewed and edited the manuscript.

### Funding

This study was funded by ALF Västerbotten Läns Landsting (ALFVLL-369861 to L.A.M.-R. [http://fou.nu/info/index.php/vll/Om\\_oss](http://fou.nu/info/index.php/vll/Om_oss)), Swedish Medical Research Council (2014-3241 to L.A.M.-R., <https://vr.se>), FP-7 Marie Curie Action “Nano-Guard” (269138 to I.A.I. and L.A.M.-R.), and Insamlingsstiftelsen (FS 2.1.12-1605-14 to L.A.M.-R., <http://www.medfak.umu.se/forskning/insamlingsstiftelsen/>).

### Notes

The authors declare no competing financial interest.

## ■ REFERENCES

- (1) Knowles, T. P. J., Vendruscolo, M., and Dobson, C. M. (2014) The amyloid state and its association with protein misfolding diseases. *Nat. Rev. Mol. Cell Biol.* 15, 384–396.
- (2) Selkoe, D. J. (2000) Toward a comprehensive theory for Alzheimer's disease. Hypothesis: Alzheimer's disease is caused by the cerebral accumulation and cytotoxicity of amyloid beta-protein. *Ann. N. Y. Acad. Sci.* 924, 17–25.
- (3) Chitnis, T., and Weiner, H. L. (2017) CNS inflammation and neurodegeneration. *J. Clin. Invest.* 127, 3577–3587.
- (4) Gandy, S., and Heppner, F. L. (2013) Microglia as dynamic and essential components of the amyloid hypothesis. *Neuron* 78, 575–577.
- (5) Blennow, K., Hardy, J., and Zetterberg, H. (2012) The neuropathology and neurobiology of traumatic brain injury. *Neuron* 76, 886–899.
- (6) in 't Veld, B. A., Ruitenber, A., Hofman, A., Launer, L. J., van Duijn, C. M., Stijnen, T., Breteler, M. M., and Stricker, B. H. (2001) Nonsteroidal antiinflammatory drugs and the risk of Alzheimer's disease. *N. Engl. J. Med.* 345, 1515–1521.
- (7) Cole, G. M., and Frautschy, S. A. (2010) Mechanisms of action of non-steroidal anti-inflammatory drugs for the prevention of Alzheimer's disease. *CNS Neurol. Disord.: Drug Targets* 9, 140–148.
- (8) McGeer, E. G., and McGeer, P. L. (2010) Neuroinflammation in Alzheimer's disease and mild cognitive impairment: a field in its infancy. *J. Alzheimer's Dis.* 19, 355–361.
- (9) Rogers, J., and Lue, L. F. (2001) Microglial chemotaxis, activation, and phagocytosis of amyloid beta-peptide as linked phenomena in Alzheimer's disease. *Neurochem. Int.* 39, 333–340.
- (10) Grathwohl, S. A., Kalin, R. E., Bolmont, T., Prokop, S., Winkelmann, G., Kaeser, S. A., Odenthal, J., Radde, R., Eldh, T., Gandy, S., Aguzzi, A., Staufenbiel, M., Mathews, P. M., Wolburg, H., Heppner, F. L., and Jucker, M. (2009) Formation and maintenance of Alzheimer's disease beta-amyloid plaques in the absence of microglia. *Nat. Neurosci.* 12, 1361–1363.
- (11) Park, K. M., Yule, D. I., and Bowers, W. J. (2008) Tumor necrosis factor-alpha potentiates intraneuronal  $\text{Ca}^{2+}$  signaling via regulation of the inositol 1,4,5-trisphosphate receptor. *J. Biol. Chem.* 283, 33069–33079.
- (12) Yoshiyama, Y., Higuchi, M., Zhang, B., Huang, S. M., Iwata, N., Saito, T. C., Maeda, J., Suhara, T., Trojanowski, J. Q., and Lee, V. M. (2007) Synapse loss and microglial activation precede tangles in a P301S tauopathy mouse model. *Neuron* 53, 337–351.
- (13) Vogl, T., Tenbrock, K., Ludwig, S., Leukert, N., Ehrhardt, C., van Zoelen, M. A., Nacken, W., Foell, D., van der Poll, T., Sorg, C., and Roth, J. (2007) Mrp8 and Mrp14 are endogenous activators of Toll-

like receptor 4, promoting lethal, endotoxin-induced shock. *Nat. Med.* 13, 1042–1049.

(14) Wang, C., Klechikov, A. G., Gharibyan, A. L., Warmlander, S. K., Jarvet, J., Zhao, L., Jia, X., Narayana, V. K., Shankar, S. K., Olofsson, A., Brannstrom, T., Mu, Y., Graslund, A., and Morozova-Roche, L. A. (2014) The role of pro-inflammatory S100A9 in Alzheimer's disease amyloid-neuroinflammatory cascade. *Acta Neuropathol.* 127, 507–522.

(15) Fritz, G., Botelho, H. M., Morozova-Roche, L. A., and Gomes, C. M. (2010) Natural and amyloid self-assembly of S100 proteins: structural basis of functional diversity. *FEBS J.* 277, 4578–4590.

(16) Schluesener, H. J., Kreamer, P. G., and Meyermann, R. (1998) Widespread expression of MRP8 and MRP14 in human cerebral malaria by microglial cells. *Acta Neuropathol.* 96, 575–580.

(17) Postler, E., Lehr, A., Schluesener, H., and Meyermann, R. (1997) Expression of the S-100 proteins MRP-8 and -14 in ischemic brain lesions. *Glia* 19, 27–34.

(18) Engel, S., Schluesener, H., Mittelbronn, M., Seid, K., Adjodah, D., Wehner, H. D., and Meyermann, R. (2000) Dynamics of microglial activation after human traumatic brain injury are revealed by delayed expression of macrophage-related proteins MRP8 and MRP14. *Acta Neuropathol.* 100, 313–322.

(19) Ha, T. Y., Chang, K. A., Kim, J., Kim, H. S., Kim, S., Chong, Y. H., and Suh, Y. H. (2010) S100a9 knockdown decreases the memory impairment and the neuropathology in Tg2576 mice, AD animal model. *PLoS One* 5, e8840.

(20) Lodeiro, M., Puerta, E., Ismail, M. A., Rodriguez-Rodriguez, P., Ronnback, A., Codita, A., Parrado-Fernandez, C., Maioli, S., Gil-Bea, F., Merino-Serrais, P., and Cedazo-Minguez, A. (2017) Aggregation of the Inflammatory S100A8 Precedes Abeta Plaque Formation in Transgenic APP Mice: Positive Feedback for S100A8 and Abeta Productions. *J. Gerontol., Ser. A* 72, 319–328.

(21) Botelho, H. M., Leal, S. S., Cardoso, I., Yanamandra, K., Morozova-Roche, L. A., Fritz, G., and Gomes, C. M. (2012) S100A6 Amyloid Fibril Formation Is Calcium-modulated and Enhances Superoxide Dismutase-1 (SOD1) Aggregation. *J. Biol. Chem.* 287, 42233–42242.

(22) Carvalho, S. B., Botelho, H. M., Leal, S. S., Cardoso, I., Fritz, G., and Gomes, C. M. (2013) Intrinsically Disordered and Aggregation Prone Regions Underlie  $\beta$ -Aggregation in S100 Proteins. *PLoS One* 8, e76629.

(23) Yanamandra, K., Alexeyev, O., Zamotin, V., Srivastava, V., Shchukarev, A., Brorsson, A. C., Tartaglia, G. G., Vogl, T., Kayed, R., Wingsle, G., Olsson, J., Dobson, C. M., Bergh, A., Elgh, F., and Morozova-Roche, L. A. (2009) Amyloid formation by the pro-inflammatory S100A8/A9 proteins in the ageing prostate. *PLoS One* 4, e5562.

(24) Eremenko, E., Ben-Zvi, A., Morozova-Roche, L. A., and Raveh, D. (2013) Aggregation of human S100A8 and S100A9 amyloidogenic proteins perturbs proteostasis in a yeast model. *PLoS One* 8, e58218.

(25) Iashchishyn, I. A., Sulskis, D., Nguyen Ngoc, M., Smirnovas, V., and Morozova-Roche, L. A. (2017) Finke-Watzky Two-Step Nucleation-Autocatalysis Model of S100A9 Amyloid Formation: Protein Misfolding as "Nucleation" Event. *ACS Chem. Neurosci.* 8, 2152–2158.

(26) Sipos, E., Kurunczi, A., Feher, A., Penke, Z., Fulop, L., Kasza, A., Horvath, J., Horvat, S., Veszelka, S., Balogh, G., Kurti, L., Eros, I., Szabo-Revesz, P., Parducz, A., Penke, B., and Deli, M. A. (2010) Intranasal delivery of human beta-amyloid peptide in rats: effective brain targeting. *Cell. Mol. Neurobiol.* 30, 405–413.

(27) Gruden, M. A., Davydova, T. V., Narkevich, V. B., Fomina, V. G., Wang, C., Kudrin, V. S., Morozova-Roche, L. A., and Sewell, R. D. (2014) Intranasal administration of alpha-synuclein aggregates: a Parkinson's disease model with behavioral and neurochemical correlates. *Behav. Brain Res.* 263, 158–168.

(28) Gruden, M. A., Davydova, T. V., Narkevich, V. B., Fomina, V. G., Wang, C., Kudrin, V. S., Morozova-Roche, L. A., and Sewell, R. D. (2015) Noradrenergic and serotonergic neurochemistry arising from intranasal inoculation with alpha-synuclein aggregates which incite parkinsonian-like symptoms. *Behav. Brain Res.* 279, 191–201.

(29) Gruden, M. A., Davydova, T. V., Wang, C., Narkevich, V. B., Fomina, V. G., Kudrin, V. S., Morozova-Roche, L. A., and Sewell, R. D. (2016) The misfolded pro-inflammatory protein S100A9 disrupts memory via neurochemical remodelling instigating an Alzheimer's disease-like cognitive deficit. *Behav. Brain Res.* 306, 106–116.

(30) During, M. J., Cao, L., Zuzga, D. S., Francis, J. S., Fitzsimons, H. L., Jiao, X., Bland, R. J., Klugmann, M., Banks, W. A., Drucker, D. J., and Haile, C. N. (2003) Glucagon-like peptide-1 receptor is involved in learning and neuroprotection. *Nat. Med.* 9, 1173–1179.

(31) Thorne, R. G., Pronk, G. J., Padmanabhan, V., and Frey, W. H., 2nd (2004) Delivery of insulin-like growth factor-I to the rat brain and spinal cord along olfactory and trigeminal pathways following intranasal administration. *Neuroscience* 127, 481–496.

(32) Illum, L. (2004) Is nose-to-brain transport of drugs in man a reality? *J. Pharm. Pharmacol.* 56, 3–17.

(33) Elder, G. A., Gama Sosa, M. A., and De Gasperi, R. (2010) Transgenic mouse models of Alzheimer's disease. *Mt. Sinai J. Med.* 77, 69–81.

(34) Sturchler-Pierrat, C., Abramowski, D., Duke, M., Wiederhold, K. H., Mistl, C., Rothacher, S., Ledermann, B., Burki, K., Frey, P., Paganetti, P. A., Waridel, C., Calhoun, M. E., Jucker, M., Probst, A., Staufenbiel, M., and Sommer, B. (1997) Two amyloid precursor protein transgenic mouse models with Alzheimer disease-like pathology. *Proc. Natl. Acad. Sci. U. S. A.* 94, 13287–13292.

(35) Xiong, H., Callaghan, D., Wodzinska, J., Xu, J., Premyslova, M., Liu, Q. Y., Connelly, J., and Zhang, W. (2011) Biochemical and behavioral characterization of the double transgenic mouse model (APP<sup>swe</sup>/PS1<sup>dE9</sup>) of Alzheimer's disease. *Neurosci. Bull.* 27, 221–232.

(36) Bryan, K. J., Lee, H., Perry, G., Smith, M. A., and Casadesu, G. (2009) Frontiers in Neuroscience, Transgenic Mouse Models of Alzheimer's Disease: Behavioral Testing and Considerations. In *Methods of Behavior Analysis in Neuroscience* (Buccafusco, J. J., Ed.), 2nd ed., CRC Press/Taylor & Francis Group, LLC, Boca Raton, FL.

(37) Kuo, Y. M., Kokjohn, T. A., Beach, T. G., Sue, L. I., Brune, D., Lopez, J. C., Kalback, W. M., Abramowski, D., Sturchler-Pierrat, C., Staufenbiel, M., and Roher, A. E. (2001) Comparative analysis of amyloid-beta chemical structure and amyloid plaque morphology of transgenic mouse and Alzheimer's disease brains. *J. Biol. Chem.* 276, 12991–12998.

(38) Van Dam, D., and De Deyn, P. P. (2011) Animal models in the drug discovery pipeline for Alzheimer's disease. *Br. J. Pharmacol.* 164, 1285–1300.

(39) Kim, H. Y., Lee, D. K., Chung, B. R., Kim, H. V., and Kim, Y. (2016) Intracerebroventricular Injection of Amyloid-beta Peptides in Normal Mice to Acutely Induce Alzheimer-like Cognitive Deficits. *J. Visualized Exp.* 109, e53308.

(40) Carulla, N., Caddy, G. L., Hall, D. R., Zurdo, J., Gairi, M., Feliz, M., Giralt, E., Robinson, C. V., and Dobson, C. M. (2005) Molecular recycling within amyloid fibrils. *Nature* 436, 554–558.

(41) Michaels, T. C., Lazell, H. W., Arosio, P., and Knowles, T. P. (2015) Dynamics of protein aggregation and oligomer formation governed by secondary nucleation. *J. Chem. Phys.* 143, 054901.

(42) Westermark, P., and Westermark, G. T. (2013) Seeding and Cross-seeding in Amyloid Diseases. In *Proteopathic Seeds and Neurodegenerative Diseases* (Jucker, M., and Christen, Y., Eds.), pp 47–60, Springer, Berlin, Heidelberg.

(43) Smith, E. E., and Greenberg, S. M. (2009) Beta-amyloid, blood vessels, and brain function. *Stroke* 40, 2601–2606.

(44) Nakagawa, S., and Cuthill, I. C. (2007) Effect size, confidence interval and statistical significance: a practical guide for biologists. *Biol. Rev. Camb. Philos. Soc.* 82, 591–605.

(45) Cliff, N. (1993) Dominance statistics: Ordinal analyses to answer ordinal questions. *Psychol. Bull.* 114, 494–509.

(46) Cohen, J. (1988) *Statistical power analysis for the behavioral sciences*, L. Erlbaum Associates, Hillsdale, NJ.

(47) Kummer, M. P., Vogl, T., Axt, D., Griep, A., Vieira-Saecker, A., Jessen, F., Gelpi, E., Roth, J., and Heneka, M. T. (2012) MRP14 deficiency ameliorates amyloid beta burden by increasing microglial

phagocytosis and modulation of amyloid precursor protein processing. *J. Neurosci.* 32, 17824–17829.

(48) Shepherd, C. E., Goyette, J., Utter, V., Rahimi, F., Yang, Z., Geczy, C. L., and Halliday, G. M. (2006) Inflammatory S100A9 and S100A12 proteins in Alzheimer's disease. *Neurobiol. Aging* 27, 1554–1563.

(49) Swindell, W. R., Johnston, A., Xing, X., Little, A., Robichaud, P., Voorhees, J. J., Fisher, G., and Gudjonsson, J. E. (2013) Robust shifts in S100a9 expression with aging: a novel mechanism for chronic inflammation. *Sci. Rep.* 3, 1215.

(50) Horvath, I., Jia, X., Johansson, P., Wang, C., Moskalenko, R., Steinau, A., Forsgren, L., Wagberg, T., Svensson, J., Zetterberg, H., and Morozova-Roche, L. A. (2016) Pro-inflammatory S100A9 Protein as a Robust Biomarker Differentiating Early Stages of Cognitive Impairment in Alzheimer's Disease. *ACS Chem. Neurosci.* 7, 34–39.

(51) Kim, H. J., Chang, K. A., Ha, T. Y., Kim, J., Ha, S., Shin, K. Y., Moon, C., Nacken, W., Kim, H. S., and Suh, Y. H. (2014) S100A9 knockout decreases the memory impairment and neuropathology in crossbreed mice of Tg2576 and S100A9 knockout mice model. *PLoS One* 9, e88924.

(52) Narumi, K., Miyakawa, R., Ueda, R., Hashimoto, H., Yamamoto, Y., Yoshida, T., and Aoki, K. (2015) Proinflammatory Proteins S100A8/S100A9 Activate NK Cells via Interaction with RAGE. *J. Immunol.* 194, 5539–5548.

(53) Ma, L., Sun, P., Zhang, J. C., Zhang, Q., and Yao, S. L. (2017) Proinflammatory effects of S100A8/A9 via TLR4 and RAGE signaling pathways in BV-2 microglial cells. *Int. J. Mol. Med.* 40, 31–38.

(54) Bucciantini, M., Calloni, G., Chiti, F., Formigli, L., Nosi, D., Dobson, C. M., and Stefani, M. (2004) Prefibrillar Amyloid Protein Aggregates Share Common Features of Cytotoxicity. *J. Biol. Chem.* 279, 31374–31382.

(55) Yan, S. D., Chen, X., Fu, J., Chen, M., Zhu, H., Roher, A., Slattery, T., Zhao, L., Nagashima, M., Morser, J., Migheli, A., Nawroth, P., Stern, D., and Schmidt, A. M. (1996) RAGE and amyloid-beta peptide neurotoxicity in Alzheimer's disease. *Nature* 382, 685–691.

(56) Haupt, C., Bereza, M., Kumar, S. T., Kieninger, B., Morgado, I., Hortschansky, P., Fritz, G., Rocken, C., Horn, U., and Fandrich, M. (2011) Pattern recognition with a fibril-specific antibody fragment reveals the surface variability of natural amyloid fibrils. *J. Mol. Biol.* 408, 529–540.

(57) Kaye, R., Head, E., Sarsoza, F., Saing, T., Cotman, C. W., Nacula, M., Margol, L., Wu, J., Breydo, L., Thompson, J. L., Rasool, S., Gurlo, T., Butler, P., and Glabe, C. G. (2007) Fibril specific, conformation dependent antibodies recognize a generic epitope common to amyloid fibrils and fibrillar oligomers that is absent in prefibrillar oligomers. *Mol. Neurodegener.* 2, 18.

(58) Goldberg, E. L., Asher, J. L., Molony, R. D., Shaw, A. C., Zeiss, C. J., Wang, C., Morozova-Roche, L. A., Herzog, R. I., Iwasaki, A., and Dixit, V. D. (2017) beta-Hydroxybutyrate Deactivates Neutrophil NLRP3 Inflammation to Relieve Gout Flares. *Cell Rep.* 18, 2077–2087.

(59) Fung, J., Frost, D., Chakrabarty, A., and McLaurin, J. (2004) Interaction of human and mouse Aβ peptides. *J. Neurochem.* 91, 1398–1403.

(60) Vogl, T., Leukert, N., Barczyk, K., Strupat, K., and Roth, J. (2006) Biophysical characterization of S100A8 and S100A9 in the absence and presence of bivalent cations. *Biochim. Biophys. Acta, Mol. Cell Res.* 1763, 1298–1306.

(61) Yamada, K., Santo-Yamada, Y., and Wada, K. (2003) Stress-induced impairment of inhibitory avoidance learning in female neuromedin B receptor-deficient mice. *Physiol. Behav.* 78, 303–309.

(62) Akar, F., Mutlu, O., Celikyurt, I. K., Bektas, E., Tanyeri, P., Ulak, G., and Erden, F. (2014) Effects of 7-NI and ODQ on memory in the passive avoidance, novel object recognition, and social transmission of food preference tests in mice. *Med. Sci. Monit. Basic Res.* 20, 27–35.

(63) Glass, G., Papin, J. A., and Mandell, J. W. (2009) SIMPLE: a sequential immunoperoxidase labeling and erasing method. *J. Histochem. Cytochem.* 57, 899–905.

(64) Pirici, D., Mogoanta, L., Kumar-Singh, S., Pirici, I., Margaritescu, C., Simionescu, C., and Stanescu, R. (2009) Antibody Elution Method for Multiple Immunohistochemistry on Primary Antibodies Raised in the Same Species and of the Same Subtype. *J. Histochem. Cytochem.* 57, 567–575.

(65) DiCiccio, T. J., and Efron, B. (1996) Bootstrap confidence intervals. *Statist. Sci.* 11, 189–228.

(66) Efron, B., and Tibshirani, R. J. (1993) *An introduction to the bootstrap*, Chapman & Hall, New York.